EFFECT OF RADIAL HEAT TRANSFER IN THE PEBBLE BED THERMAL ENERGY STORAGE TANK COUPLED TO A SOLAR ORGANIC RANKINE CYCLE

Pardeep Garg[1*], Abhishek N. Kshirsagar[2], Pramod Kumar[1#], Matthew S. Orosz[4]

[1] Indian Institute of Science Bangalore
C V Raman Ave, Bengaluru, Karnataka, India
[*]E-mail: pardeep_1127@yahoo.com
[#]E-mail: pramod_k24@yahoo.com

[2] Pune Vidyarthi Griha's College of Engineering and Technology
Vidyanagari, Pune, Maharashtra, India
E-mail: kshirsagar_abhishek@yahoo.com

[4] Massachusetts Institute of Technology
Cambridge, Boston, USA
E-mail: mso@mit.edu

ABSTRACT

This paper analyzes the heat transfer mechanisms in the pebble-bed storage medium and reports the issues associated with it. A cylindrical geometry is considered for the storage tank in the present analysis for three different geometrical configurations which are solved using CFD commercial solver, Fluent 6.0, ANSYS. These configurations have different positions for inlet and outlet ports, namely, a) central inlet and outlet configuration (C-IOC), b) uniform inlet and outlet configuration (U-IOC) and c) diametrically opposite inlet and outlet ports on the lateral surface or the side inlet and outlet configuration (S-IOC) of the cylindrical TES tank. A comparative analysis of these three configurations is presented and internal heat transfer issues in the radial direction are identified. A new parameter called effectiveness of the TES tank is proposed to quantify the energy stored in the tank at the end charging process. Finally, the side inlet and outlet case is found to be a practically realizable as well as an effective alternate.

1. INTRODUCTION

Thermal energy storage (TES) is one of means of suppressing the adverse effects arising due to solar fluctuations on the power cycles and is also recognized as a cheaper option to store energy to generate electricity during non-solar hours (Taljan *et al.*, 2012). There are a number ways in which energy can be stored for example in form of sensible and latent heat. Herrmann and Kearney (2002) optimized these technologies on the basis of techno-economic analysis and emphasized on the need of reducing the cost of storage media. One possible way to reduce the cost of storage medium is to store partial amount of heat in the inexpensive rocks or pebbles as suggested by Meier et al. (1991). Pertaining to this, the economic advantages of pebble-bed TES (PB-TES) have been established by Zavattoni *et al.* (2013).Various studies have been made for understanding the heat storage mechanisms in these systems by modeling the heat transfer processes in it. For example, Ismail and Stuginsky (1999) modeled packed bed as porous media, Shah and Furbo (2003) analyzed the heat transfer fluid (HTF) entrance effects into the tank and Benmasour *et al.* (2006) treated uniformly sized spherical capsules as pebble bed in a two dimensional computational domain. These models are generally simplified and do not capture temperature gradients in the radial direction. However, the present paper finds that these effects can significantly lower the heat storage potential in a PB-TES system and hence the same need to be accounted for in the governing equations. Further, various inlet and outlet configurations of the PB-TES system are considered to show their effect on the energy stored in a given PB-TES system and in a given charging time.

2. SOLAR-ORC DETAILS AND CASE STUDY

Physical layout of the solar-ORC considered in this paper consists of two closed loops, a) heat transfer fluid (HTF) and b) working fluid loop as shown in Fig. 1. In the HTF loop, cold HTF from a PB-TES is pumped to a parabolic trough collector where it gets heated up and is then sent for the storage in a PB-TES tank. Working fluid loop is a regenerative ORC where the expander exhaust heat is recovered to heat up the pump outlet fluid. The two loops interact via a heat exchanger termed as an HEX (boiler for the working fluid) in this paper where the HTF coming from a PB-TES tank is cooled and working fluid in turn is heated up to the expander inlet temperature. TES is modeled in such a way that temperature drop across the HTF in HEX and PB-TES are identical.

2.2 TES details

Heated HTF from solar field enters the PB-TES tank from the inlet port (at or near the top) where it loses heat to the pebbles and the cold HTF around. The same amount of cold HTF leaves the tank from the outlet port (at or near the bottom) and is passed to the solar collectors to heat it up again. The process of storing heat from the solar collectors is termed as charging of the PB-TES whereas utilizing of the heat from the PB-TES in the power block is called discharging of the tank. In a real scenario, both the processes occur simultaneously and the one dominating over the other decides the net energy stored at any instance in the tank. To simplify the actual phenomenon occurring in the tank, only the charging process is simulated in this paper to understand the effect of location of inlet and outlet ports on a PB-TES. Schematics of these configurations are shown in Figure 2.

2.1 Case study

A detailed study of heat transfer mechanisms in a PB-TES system is carried out for a solar-ORC yielding a steady output of 100 kWe for the duration 600 Hrs. to 1800 Hrs. The working fluid used in the ORC is R-134a operating between 175 ºC and 45 °C with the expander inlet pressure of 52 bar (transcritical cycle) optimized for maximum efficiency equal to ~10 %. Details of cycle modeling can be found in Garg *et al*., (2013). HTF operating temperatures across the boiler are found to be 358 and 438 K. Location selected for study of the solar and DNI characteristics is 23.5°, 80° (latitude chosen is Tropic of Cancer which represents roughly the average of extreme Indian latitudes) and the day chosen is Vernal Equinox. The TES system selected is a pebble-bed system with fused silica as the pebble material and ethylene glycol as the HTF with their thermo-physical properties mentioned in section 3. Various assumptions made regarding the tank are listed below.

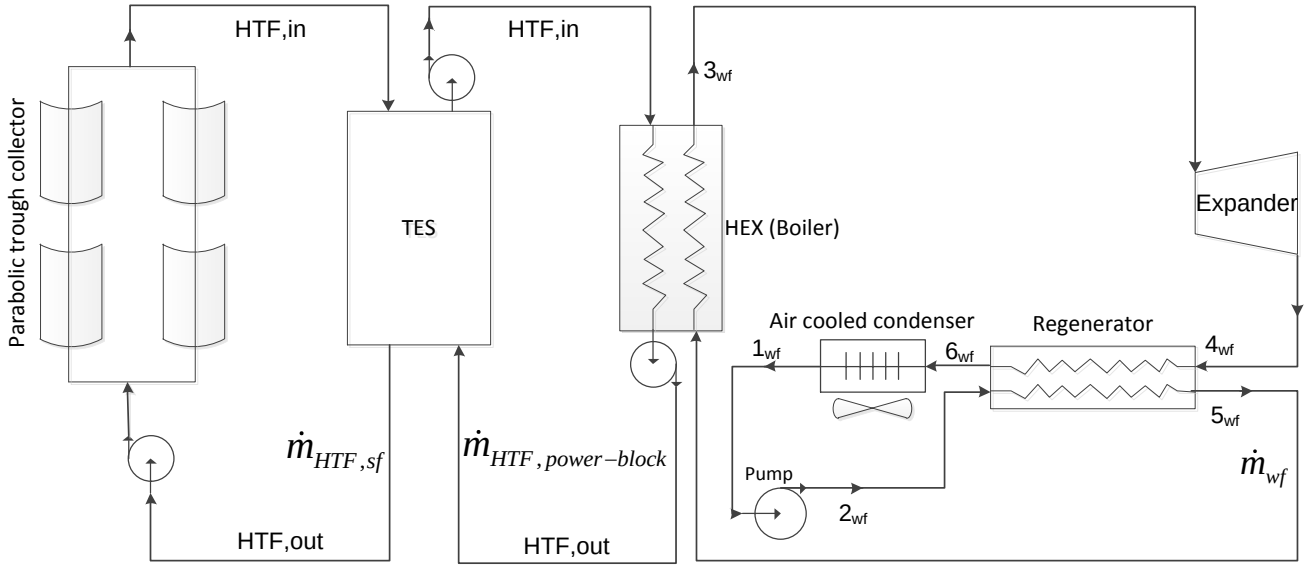

Fig 1: Schematic of an ORC coupled to parabolic trough collector

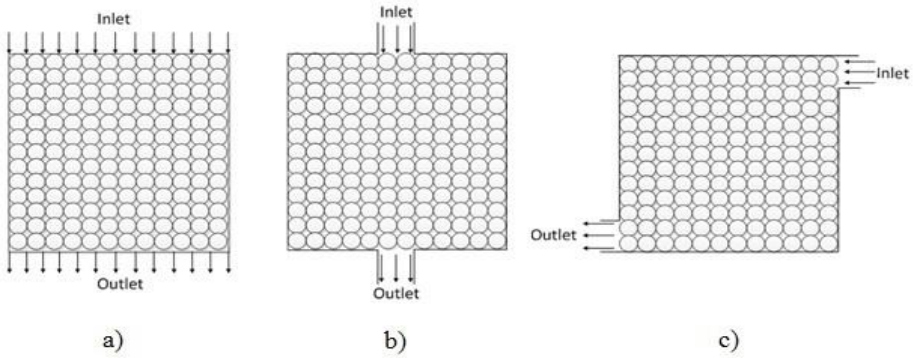

Figure 2: Schematic representation of cross-section at inlets and outlets of all the configurations

Assumptions:

i. Control strategy followed in the solar field is the regulation of mass flow rate to achieve steady $T_{HTF,in}$. However, for the simulation purposes, mass flow rate across the PB-TES is averaged out and assumed to be constant during the charging process.

ii. Though, thermo-physical properties of HTF are assumed to be the function of temperature as given in the section 3, for the given operating conditions of HTF, these are taken to be the average of those at $T_{HTF,mean}$ defined as

$$T_{HTF,mean} = \frac{T_{HTF,in} + T_{HTF,out}}{2} \tag{1}$$

iii. The porosity (φ) is 0.45 and the geometry selected has an aspect ratio ($L_{PB\text{-}TES}/D_{PB\text{-}TES}$) of unity.

iv. TES has adiabatic walls.

3. METHODOLOGY

The basic methodology for PB-TES sizing is given in detail in Kshirsagar *et al.*(2015), but the salient features are repeated for the sake of completeness of this paper in Appendix A. PB-TES with uniformly sized spherical balls is modeled as a porous media in Fluent 6.0 and the following governing equations are solved to capture heat transfer issues in radial direction.

$$\varphi \frac{\partial \rho_f}{\partial t} + \nabla.(\rho_f \, \mathrm{v}) = 0 \tag{2}$$

$$\rho_f \left[\frac{1}{\varphi} \frac{\partial \mathrm{v}}{\partial t} + \frac{\mathrm{v}}{\varphi} \nabla \left(\frac{\mathrm{v}}{\varphi} \right) \right] = -\nabla P + \frac{\mu}{\varphi p_f} \nabla^2 \mathrm{v} - \frac{\mu}{K} \mathrm{v} \tag{3}$$

$$\left((1-\varphi)(\rho \mathrm{c})_s + \varphi (\rho \mathrm{c}_p)_f \right) \frac{\partial T}{\partial t} + (\rho c_p)_f \nabla T = \nabla.(k_s \nabla T) + \varphi \nabla.\nabla T (k_f - k_s) \tag{4}$$

Condition of local thermal equilibrium is assumed to prevail in the tank in the above equation. Also, the flow considered here is laminar as the Reynolds number is well within its range (~400). The HTF inlet is chosen as velocity inlet. The internal surface or volume is selected as porous zone. The walls are chosen as stationary with a no slip condition (Versteeg and Malalasekera, 2007). Viscous resistance in all the directions calculated using Darcy's law and Ergun's equation comes out to be $4.878 \times 10^6 \mathrm{m}^{-2}$. The thermo-physical properties of fused silica and ethylene glycol are as follows:

Properties	Ethylene glycol	Fused silica
Density, ρ (kg/m^3)	882	2200
Specific heat, C_p (J/kgK)	3000	740
Thermal conductivity, K (W/mK)	0.1951	1.3
Dynamic viscosity, μ (Pa.s)	6.535×10^{-4}	-

Table 1: Thermo-physical properties of ethylene glycol as HTF and fused silica as pebble material

3.1 Boundary conditions

The mass flow rate during the charging process at the inlet and the outlet is taken as 0.6846 kg/s. The inlet temperature is chosen as 438 K and the tank is initially kept at 358 K. An 'outflow' boundary condition is used for the HTF outlet since the details of flow velocities and pressure are not known prior to solving the flow problem (Ansys Inc., 2009). The C-IOC and the U-IOC are axisymmetric in nature and are likewise simulated. The S-IOC is simulated as a three dimensional geometry. The simulation is done for the charging process during excess period of the day. Table 1 shows different characteristics of tank for all the IOCs. The inlet and outlet diameters of ports are so chosen in order to minimize the pressure drop across unit length of the tube to 0.1 kPa/m.

Characteristic	U-IOC	C-IOC	S-IOC
Height (m)	3.4	3.4	3.4
Diameter (m)	3.4	3.4	3.4
Porosity	0.45	0.45	0.45
IO port diameter (m)	3.4	0.4	0.4

Table 2: Characteristics of tank for different IOCs

3.2 Parameter of interest

A new parameter called effectiveness of the TES tank is introduced defined as the ratio of actual to ideal case energy stored at the end of charging process in a PB-TES system designed ignoring radial effects.

$$\varepsilon = \frac{E_{PB-TES,actual}^{t=\text{charging time}}}{E_{PB-TES,ideal}^{t=\text{charging time}}} \tag{5}$$

4. RESULTS AND DISCUSSIONS:

Three different inlet and outlet configurations namely central, uniform and the side are analyzed and compared for the given parameters as mentioned in Table 1. Firstly, U-IOC which is the closest to the ideal configuration is studied. In this case, at any instance, both the fluid and the pebbles in a horizontal plane tend to achieve local equilibrium and no temperature gradients are found. This is mainly due to the fact that all the radial positions in any plane in the tank have an equal access to flow and hence thermal energy. Thus, there are no thermally insulated corners in the tank and hence the storage potential is realized to its maximum as shown in Figure 3.

Though the U-IOC produces the best results, it is not practically realizable as the uniform distribution of fluid is hard to achieve in a real scenario. The second and most popular configuration in literature is reported to be the C-IOC. At the end of charging time (t_{full}), TES system is found to have the isolated corners in the bottom extreme of the tank as shown in Figure 4 depicting the inability of the TES to store energy to its fullest.

In both the scenarios mentioned above, the outlet is placed on the bottom of tank which needs a submersible pump leading to higher exergy losses (Pacheco et al., 2002) and a complicated system. An alternative could be to have the side inlet and outlet configuration (S-IOC) which is easily realizable and has the potential to offer better performance indicators than the central one. Temperature distribution in this case is plotted in Figure 5 at t_{full} wherein thermally isolated corners near the lateral wall are visible.

Effect of these TES configurations is then studied on the ORC performance. Further, envelope heat transfer losses are assumed to minimize the heat recovered potential by 5 %. Thus, in an ideal (U-IOC) scenario designed for a 100 kW system for a vernal equinox day, electricity collected would be around 1140 kWh. The other configurations like C-IOC and S-IOC would deliver only 912 and 997.5 kWh of electricity. These details are shown in Table 3.

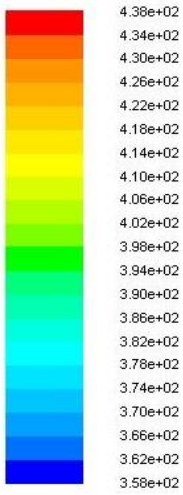

Figure 3: Contours of static temperature for U-IOC after t_{full} (left vertical axis of cylinder denotes the center of tank)

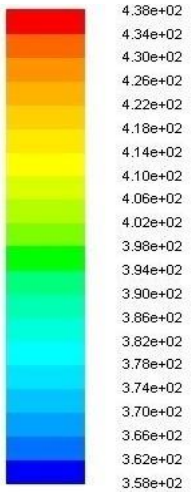

Figure 4: Contours of static temperature for C-IOC after t_{full} (left vertical axis of cylinder denotes the center of tank)

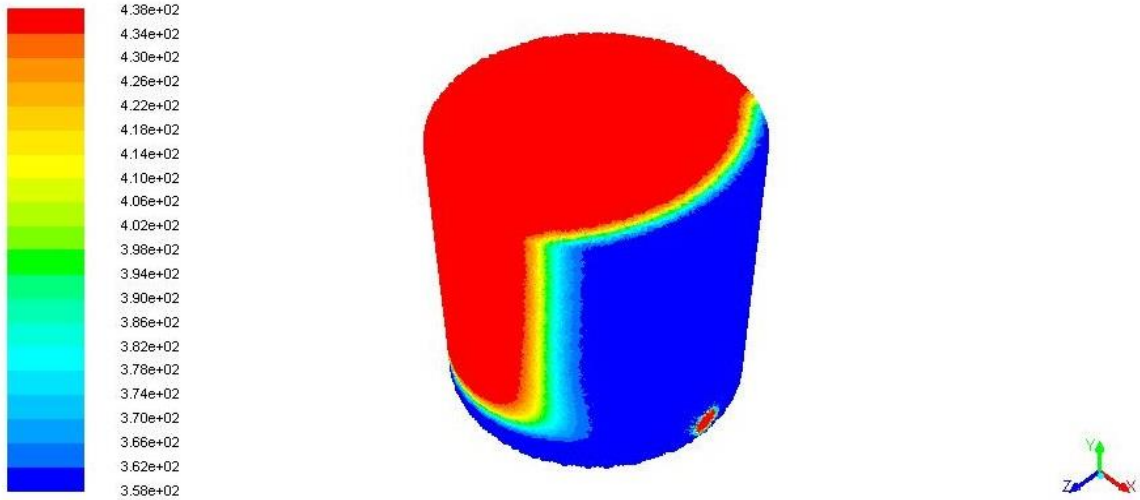

Figure 5: Contours of static temperature for S-IOC after t_{full}

Next, we perform the comparison among the three configurations on the basis of evolution of energy stored and net energy stored at t_{full}. In this regard, Figure 6 shows the variation of HTF outlet temperature with respect to flow time. It can be seen that the HTF outlet temperature in case of uniform configuration stays almost steady throughout t_{full} (358 K) except for the time when thermocline zone reaches the bottom part of the tank (~29000 s). In rest of the two cases, HTF outlet temperature starts increasing from its base value of 358 K at the instant (denoted as $t_{short\text{-}circuit}$) when the high temperature fluid is near to the bottom part of the tank resulting in isolated corners. In case of C-IOC, $t_{short\text{-}circuit}$ is found to be ~ 12000 s whereas for the side inlet and outlet case it is ~18000 s. Higher value of $t_{short\text{-}circuit}$ for the latter can be explained using the fact that HTF tends to travel more in the tank (along the diagonal) before it reaches the bottom part than in the latter where the HTF travels vertically. These indicate that the heat transfer characteristics of both the configurations are consistent with the above discussion. Finally, the figure shows the side configuration to have intermediate properties between those of the central and uniform.

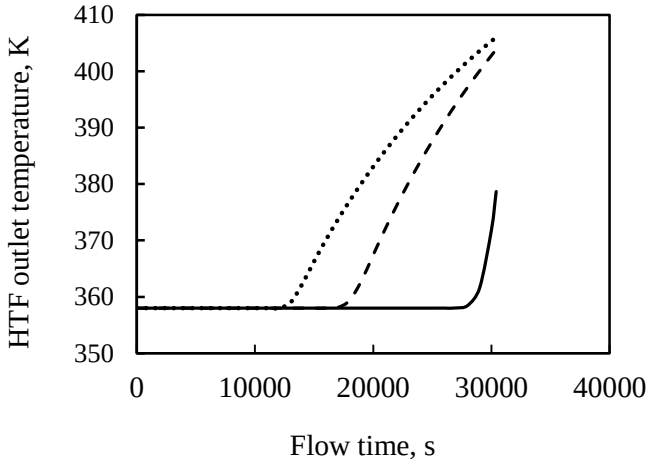

Figure 6: HTF outlet temperature versus flow time for U-IOC, S-IOC and C-IOC.
Legend: ———U-IOC,——S-IOC,·····C-IOC.

Pertaining to the figures above, energy stored in the tank with respect to flow time is plotted in figure 7. Rate at which the energy is stored remains constant with time for the U-IOC throughout the charging process. The same is not true in the other two scenarios. After $t=t_{short\text{-}circuit}$, the rate of energy storage decreases which at the end of charging time leads to the lower amount of energies stored. Further, S-IOC fares on the parameter of effectiveness which can store 87.5 % energy as compared to 80 % in the central inlet and outlet case (Table 3).

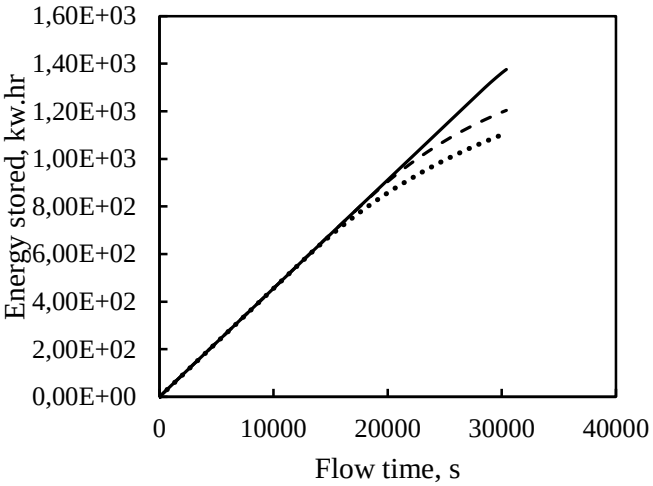

Figure 7: HTF outlet temperature versus flow time for U-IOC, S-IOC and C-IOC.
Legend: ——— U-IOC,—— S-IOC, ·····C-IOC.

Inlet and outlet configuration	Effectiveness ($\mathcal{E}$)	Energy stored per day(1200×0.95× $\mathcal{E}$)
Uniform	1	1140 kWhr
Central	0.8	912 kWhr
Side	0.875	997.5 kWhr

Table 3: Effectiveness of various IOCs

5. CONCLUSION

CFD simulation of pebble bed based thermal energy storage systems establishes the fact that temperature gradients in the radial direction can significantly affect the heat storage efficiencies which in turn are dependent on the inlet and outlet configuration. A comparative analysis of these systems with different inlet and outlet configurations is presented. The U-IOC is found to be the closest to the ideal case wherein radial temperature gradients are absent. However, practical issues like placement of the discharge pump in this scenario motivates for other alternates. Such an alternate is a configuration with S-IOC which is found to store 7.5 % higher energy than the present state of art with the C-IOC. The future scope of this work may involve rating these different TES tanks for various aspect ratios along with the modeling of simultaneous modeling of charging and discharging process.

REFERENCES

Garg P., Kumar P., Srinivasan K., Dutta P., 2013, Evaluation of carbon dioxide blends with isopentane and propane as working fluids for organic Rankine cycles, *Applied Thermal Engineering*, Vol. 52, pp 439-448.

Gregor Taljan, Gregor Verbi, Milos Pantos, Manfred Sakulin, Lothar Fickert, 2012, Optimal sizing of biomass-fired Organic Rankine Cycle CHP system with heat storage, *Renewable Energy*, vol. 41 p. 29-38

Ulf Herrmann, David W. Kearney, 2002, Survey of Thermal Energy Storage for Parabolic Trough Power Plants, *Journal of Solar Energy Engineering*, Vol. 124/145-152

G. Zanganeh, A. Pedretti, S. Zavattoni, M. Barbato, A. Steinfeld, 2012, Packed-bed thermal storage for concentrated solar power – Pilot-scale demonstration and industrial-scale design, *Solar Energy*, vol. 86 p. 3084–3098

Mawire, M. McPherson, 2009, Experimental and simulated temperature distribution of an oil-pebble Bed thermal energy storage system with a variable heat source, *Applied Thermal Engineering*, vol. 29 p. 1086–1095A.

Hasnain SM. Review on sustainable thermal energy storage technologies. Part1. Heat storage materials and techniques, *Energy Convers Manage*, J1998;39(11):1127–38

Quoilin, S., Orosz, M., Hemond, H., Lemort, V., 2011, Performance and design optimization of a low-cost solar organic Rankine cycle for remote power generation, *Solar Energy*, vol. 85, no. 5: p. 955-966.

Orosz, M. S., 2012, ThermoSolar and photovoltaic hybridization for small scale Distributed Generation: Applications for Powering Rural Health, Doctoral dissertation, Massachusetts Institute of Technology.

Orosz, M. S., Quoilin, S., Hemond, H., Sorce: A Design Tool For Solar Organic Rankine Cycle Systems In Distributed Generation Applications

Curran, H. M., 1993, Mechanical systems and components, *In:*Lof, G. O. G., *Active Solar Systems*, MIT Press, Cambridge, MA: p. 693-743

Appendix A

Following steps are used to calculate mass of HTF required operating ORC at its steady operating conditions

a) Energy stored in the TES
The rate at which the energy is available to the TES from the collector is given by eq. 1.

$$\dot{Q}_{collector} = \eta_{collector} DNI_N A_{collector} \tag{A.1}$$

Heat required in power block is given by

$$\dot{Q}_{power-block} = \frac{\dot{P}}{n_{ORC}} \tag{A.2}$$

Also, area (ABCD) = area (AGHD) for the continuous operation of power block for Δt_h time

$$\dot{Q}_{power-block} \Delta t_h = \int_{t_{1h}}^{t_{4h}} \dot{Q}_{collector} dt_h \tag{A.3}$$

It can be noted that heat available from the collector exceeds that of required in the power block in the hours between t_{2h} to t_{3h} and can be stored in the PB-TES. The stored heat can then later be used in the hours between t_{1h} to t_{2h} and t_{3h} to t_{4h} when the heat available from the collector is not enough to run the power block. It can be seen that the heat stored in the surplus hours should be equal to energy used in the deficit hours for the steady operation of power block. Energy that need to be stored in the PB-TES is thus given as

$$\Delta E_{PB-TES} = \text{area}(arc(BC)) - \text{area}(BCFE) \tag{A.4}$$

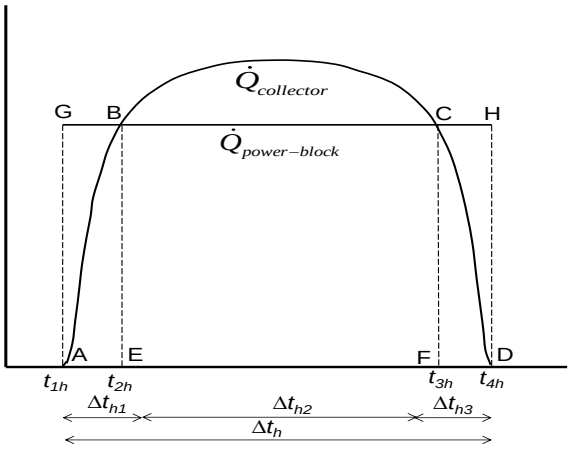

Figure A.1 Plot of a typical DNI profile with a constant power output

Eq.3 can be used to calculate the area of collector required. Eqs. (A.1) and (A.2) are plotted in Fig. 3.

$$\Delta E_{PB-TES} = \text{area}(arc(BC)) - \text{area}(BCFE) \tag{A.5a}$$

Or

$$\Delta E_{PB-TES} = \int_{t_{2h}}^{t_{3h}} \dot{Q}_{collector} dt_h - \dot{Q}_{power-block} \Delta t_{3h} \tag{A.5b}$$

b) Mass of HTF stored in PB-TES
Total energy stored in the PB-TES is given by

$$\Delta E_{PB-TES} = \Delta E_{HTF} + \Delta E_{Pebble} \quad \text{(A.6)}$$

Where,

$$\Delta E_{HTF} = M_{HTF} c_{p_{HTF}} \Delta T_{HTF} \quad \text{(A.7)}$$

$$\Delta E_{Pebble} = M_{Pebble} c_{p_{Pebble}} \Delta T_{Pebble} \quad \text{(A.8)}$$

Condition of local thermal equilibrium is assumed to be persistent in the PB-TES making the temperature of HTF and pebble equal.

PB-TES can be modeled as a porous media with porosity or void fraction equal to φ where,

$$\varphi = \frac{V_{HTF}}{V_{Total}} \quad \text{(A.9)}$$

Where V_{Total} and V_{HTF} is the volume of the PB-TES.

V_{Total} can be calculated from the above equation.

$$\Delta E_{PB-TES} = (\varphi \rho_{HTF} c_{p_{HTF}} + (1-\varphi)\rho_{Pebble} c_{p_{Pebble}}) V_{Total} \Delta T_{HTF} \quad \text{(A.10)}$$

Using Eqs. (B.7), (B.10) and (B.4), M_{HTF} can be simplified to

$$M_{HTF} = \frac{\Delta E_{PB-TES}}{c_{p_{HTF}} \Delta T_{HTF}} - M_{Pebble} \frac{c_{p_{Pebble}}}{c_{p_{HTF}}} \quad \text{(A.11)}$$

Above equation establishes an inverse relationship between M_{HTF} and ΔT_{HTF}.

NOMENCLATURE

l	Latitude	(º)
ω	Hour angle	(º)
n	Day number	(-)
δ	Declination	(º)
β	Solar altitude angle	(º)
φ	Solar azimuth angle	(º)
γ	Surface solar azimuth angle	(º)
θ	Angle of incidence	(º)
α	Tilt angle	(º)
A	Apparent solar irradiation at air mass equal to zero	(W/m^2)

B	Atmospheric extinction coefficient	(-)
C_N	Clearness number	(-)
T	Temperature	(K)
M	Mass	(kg)
E	Energy	(J)
V	Volume	(m^3)
$A_{collector}$	Area of collector field	(m^2)
$\dot{Q}$	Power	(W)
$\dot{P}$	Output power	(W)
t	Time	(Hours)
c_p	Specific heat	(J/kgK)
η	Efficiency	(-)
ρ	Density	(kg/m^3)
ε	Effectiveness	(-)
$\dot{m}$	Mass flow rate	(kg/s)
φ	Porosity	(-)
v	Seepage velocity	(m/s)
k	Thermal conductivity	(W/mK)
μ	Dynamic viscosity	(Pa.s)

Subscript

h	hour
HTF	heat transfer fluid
Pebbles	pebble
PB-TES	pebble bed thermal energy storage
power-block	power block
collector	collector
Total	total tank
f	fluid
s	solid
full	full
short-circuit	condition when HTF at 438 K reaches outlet

Abbreviations

TES	thermal energy storage
HTF	heat transfer fluid
DNI	direct normal insolation
PB-TES	pebble-bed thermal energy storage
ORC	organic Rankine cycle
IOC	inlet and outlet configuration
U-IOC	uniform inlet and outlet configuration
C-IOC	central inlet and outlet configuration
S-IOC	side inlet and outlet configuration

ACKNOWLEDGEMENT

This research is based upon work supported by the Solar Energy Research Institute for India and the U.S. (SERIIUS) funded jointly by the U.S. Department of Energy subcontract DE AC36-08G028308 (Office of Science, Office of Basic Energy Sciences, and Energy Efficiency and Renewable Energy, Solar Energy Technology Program, with support from the Office of International Affairs) and the Government of India subcontract IUSSTF/JCERDC-SERIIUS/2012 dated 22nd Nov. 2012.